fluids

MDPI

Article

Liutex for Visualization of the Tropical Cyclone Structure

Chenxi Ma [1], Yifei Yu [1], Sim D. Aberson [2], Jun A. Zhang [2,3] and Chaoqun Liu [1,*]

[1] Department of Mathematics, University of Texas at Arlington, Arlington, TX 76013, USA
[2] National Oceanic and Atmospheric Administration (NOAA)/Oceanic and Atmospheric Research (OAR)/Atlantic Oceanographic and Meteorological Laboratory/Hurricane Research Division, Miami, FL 33149, USA
[3] Department of Atmospheric Sciences, University of Miami, Miami, FL 33149, USA
* Correspondence: cliu@uta.edu

Abstract

Tropical cyclones are among the most destructive weather systems, causing substantial societal and economic impacts worldwide. Accurate visualization and identification of tropical cyclone vortex structures are essential for understanding their organization and evolution. In this study, the Liutex method, a vector-based vortex identification technique that separates rigid body rotation from shear, is applied to two representative Atlantic hurricanes, Teddy and Dorian. The performance of Liutex is compared with conventional vortex identification methods: vorticity, the Q criterion, and the λ_2 criterion. Liutex provides clear visualization of the eye, eyewall, and rainbands, enabling intuitive identification of localized regions of rigid body rotation. Furthermore, Liutex fields suggest that the eyewall and rainbands are made up of numerous localized vortical structures in the horizontal and vertical directions rather than forming a single continuous vortex ring or line, offering a new perspective on tropical cyclone organization. These findings demonstrate the potential of Liutex as a physically meaningful diagnostic and visualization tool for investigating tropical cyclone vortex structures and other complex rotating flows.

Keywords: tropical cyclone; vortex identification; Liutex; Q criterion; λ2 method

1. Introduction

Hurricanes, typhoons, and cyclones, collectively known as tropical cyclones, are characterized by destructive heavy rainfall and strong winds. A mature tropical cyclone can be divided into three regions from the center outward (the eye, eyewall, and rainbands) in the horizontal, although there are no rigorous, objective definitions to characterize distinct boundaries between them. The eye is a relatively quiescent region surrounded by the eyewall; outside the eyewall are numerous cloud lines known as rainbands. [1] Tropical cyclones have historically been characterized as regions of high vertical vorticity at low resolution; with increasing resolution, the eye, eyewall, and some rainbands can be seen, though the vertical vorticity maxima are sometimes inside these features due to horizontal shear, and sometimes a vorticity monopole exists [2]. In the vertical, complex near-surface features known as roll vortices have been hypothesized to control the interaction between the atmosphere and the ocean below that provides the fuel for tropical cyclones, and they may also be important in the upper-level outflow layer where mass is evacuated at the top of the troposphere.

Liutex is a novel physical quantity used in fluid dynamics to rigorously define and mathematically identify the local rotation, or vortex, of a fluid. It was proposed by Liu et al.

Check for updates

Academic Editor: Xavier Carton

Received: 30 July 2026
Revised: 15 September 2026
Accepted: 17 September 2026
Published: 23 September 2026

Copyright: © 2026 by the authors. Licensee MDPI, Basel, Switzerland. This article is an open access article distributed under the terms and conditions of the Creative Commons Attribution (CC BY) license.

in 2018 [3,4] as the third-generation method in vortex identification [5]. The main ideas of Liutex theory are that vorticity is a combination of rigid rotation and shear, and that the velocity gradient tensor can be decomposed into three parts: rotation, shear, and stretching or compression. In 2025, Alvarez et al. used Liutex for tropical cyclones for the first time and confirmed that they are not single vortices but systems formed by many small ones [6]. This gives us new insights into the structure of tropical cyclones and helps interpret the physical mechanisms behind cyclogenesis and changes in intensity and structure.

The present study extends this earlier work into three important aspects. First, Liutex is compared with first- and second-generation vortex identification methods (vorticity, the Q criterion, and the λ_2 criterion) using analyses of real data from multiple Atlantic hurricanes. This comparison allows for an assessment of the impact of shear in various methods. Second, the vector nature of Liutex is exploited by separately examining its vertical and horizontal components, which enables a clear identification of various tropical cyclone features. Third, Liutex core lines are used to reveal the three-dimensional organization of rotational structures within the hurricane.

The manuscript begins with a brief review of the three generations of vortex identification methods, followed by a comparison of Liutex and conventional vortex diagnostics for identifying and visualizing tropical cyclone features. The results are then used to illustrate the advantages of Liutex for characterizing tropical cyclone vortex structures and to discuss its potential applications in tropical cyclone visualization and analysis.

2. 3 Generations of Vortex Identification Methods

2.1. First Generation: Vorticity

Although vorticity is widely used to characterize rotating flows as the first-generation vortex identification method since Helmholtz proposed his 3 important hypotheses and developed vorticity theory [7], it cannot distinguish rigid body rotation from shear, motivating the development of more advanced vortex identification methods. According to Cauchy–Stokes theory [8], which is similar to Helmholtz's theory, the transpose of the velocity gradient matrix can also be decomposed into 2 parts: a symmetric strain part A and an anti-symmetric vorticity part B, which is also considered the rotational part.

$$\nabla v = \begin{pmatrix} \frac{\partial u}{\partial x} & \frac{\partial v}{\partial x} & \frac{\partial w}{\partial x} \\ \frac{\partial u}{\partial y} & \frac{\partial v}{\partial y} & \frac{\partial w}{\partial y} \\ \frac{\partial u}{\partial z} & \frac{\partial v}{\partial z} & \frac{\partial w}{\partial z} \end{pmatrix} \begin{cases} A = \frac{1}{2}\left(\nabla v^T + \nabla v\right) \\ B = \frac{1}{2}\left(\nabla v^T - \nabla v\right) \\ \nabla v^T = A + B \end{cases} \tag{1}$$

Here, u, v, and w are the three components of the velocity vector in the x, y, and z directions, respectively; ∇v is the velocity gradient matrix, a 3×3 matrix composed of 9 partial derivatives of velocity by direction. Vorticity cannot define rotation, which can be easily demonstrated using two-dimensional channel flow:

$$u = 1 - y^2;\ v = 0\ (-1 \le y \le 1) \implies |\omega| = \left|\frac{\partial u}{\partial y}\right| = 2|y|$$

Here, we can find the existence of vorticity at the boundary of the flow, which becomes large as $y \longrightarrow \pm 1$. No vortex exists since all the particles are moving in a straight line.

2.2. Second Generation: Scalar Methods

After recognizing that vorticity has limitations in identifying vortices, especially in the boundary layer where shear is strong due to viscosity, several empirical methods for vortex identification based on velocity gradients were proposed.

The Q criterion was proposed by Hunt et al. in 1988, and the idea follows the velocity gradient matrix decomposition in the Helmholtz manner [9].

$$\|B\|_F^2 = \frac{1}{2}\left[\left(\frac{\partial v}{\partial x} - \frac{\partial u}{\partial y}\right)^2 + \left(\frac{\partial w}{\partial x} - \frac{\partial u}{\partial z}\right)^2 + \left(\frac{\partial v}{\partial z} - \frac{\partial w}{\partial y}\right)^2\right]$$

$$\|A\|_F^2 = \frac{1}{2}\left[\left(\frac{\partial v}{\partial x} + \frac{\partial u}{\partial y}\right)^2 + \left(\frac{\partial w}{\partial x} + \frac{\partial u}{\partial z}\right)^2 + \left(\frac{\partial v}{\partial z} + \frac{\partial w}{\partial y}\right)^2\right] + \left[\left(\frac{\partial u}{\partial x}\right)^2 + \left(\frac{\partial v}{\partial y}\right)^2 + \left(\frac{\partial w}{\partial z}\right)^2\right]$$

$$\begin{aligned} Q = \frac{\|B\|_F^2 - \|A\|_F^2}{2} &= -\frac{\partial v}{\partial x}\frac{\partial u}{\partial y} - \frac{\partial w}{\partial x}\frac{\partial u}{\partial z} - \frac{\partial v}{\partial z}\frac{\partial w}{\partial y} - \frac{1}{2}\left[\left(\frac{\partial u}{\partial x}\right)^2 + \left(\frac{\partial v}{\partial y}\right)^2 + \left(\frac{\partial w}{\partial z}\right)^2\right] \\ &= - < \nabla v^T, \nabla v > /2 \end{aligned} \quad (2)$$

Here, '$< , >$' stands for the matrix dot product. Rotation exists when $Q > 0$, so only positive values are shown in this study.

The λ_2 method proposed by Jeong and Hussain in 1995 [10] uses the second largest eigenvalue of $A^2 + B^2$:

$$A^2 + B^2 = \frac{1}{4}\left[\left(\nabla v^T + \nabla v\right)^2 + \left(\nabla v^T - \nabla v\right)^2\right] = \frac{1}{2}\left(\nabla v^2 + \nabla v^{T^2}\right)$$

$$\lambda_2 = 0.5 \,\mathrm{med}\left(\mathrm{eigenval}\left(\nabla v^2 + \nabla v^{T^2}\right)\right) \quad (3)$$

where med and eigenval stand for the median value and the eigenvalues of the matrix, respectively. Rotation exists when $\lambda_2 < 0$, so only negative values are shown in this study.

The λ_{ci} and Δ methods [11,12] are based on the eigenvalues of the velocity gradient matrix. If the velocity gradient matrix has complex eigenvalues, then both the discriminant of the characteristic polynomial Δ, and the imaginary part of the complex eigenvalues λ_{ci} will both be positive. These two methods can find vortices, but their physical interpretation is not directly related to the rigid rotation, as is the case for the Q and λ_2 criteria.

2.3. Third Generation: Liutex Method

The third generation of vortex identification methods, Liutex, was proposed by Liu et al. in 2018 [3,4]. Unlike second-generation scalar diagnostics, Liutex is a vector quantity that provides both the magnitude and direction of local rigid body rotation [13]. Furthermore, the second-generation vortex identification methods also include shear. Because they are scalar, they must use arbitrary isosurfaces that depend on an empirical threshold selection.

The Liutex vector $\vec{R}$ can be found [14] as:

$$\vec{R} = \left[\vec{\omega}\cdot\vec{r} - \sqrt{(\vec{\omega}\cdot\vec{r})^2 - 4{\lambda_{ci}}^2}\right]\vec{r} \quad (4)$$

where $\vec{\omega} = \nabla \times \vec{v}$ is the vorticity, λ_{ci} is the imaginary part of the 2 complex eigenvalues of ∇v, and $\vec{r}$ is the eigenvector of the unique real eigenvalue of ∇v^T such that $\vec{\omega}\cdot\vec{r} > 0$. If ∇v has more than 1 real eigenvalue, then by default $\vec{R} = 0$. In this study, the vertical component (R_z) and the magnitude of the horizontal component ($R_h = \sqrt{{R_x}^2 + {R_y}^2}$) are visualized and analyzed.

2.4. Liutex Core Line Method

Liutex core lines [15] are curves that connect points at which the Liutex magnitude is a local maximum in planes normal to the local Liutex direction. Mathematically, Liutex core lines are the lines formed by the points satisfying

$$\nabla R \times \vec{r} = 0, \quad R > 0 \tag{5}$$

Liutex core lines mark the instantaneous centerlines of vortices, rather than fluid particle trajectories or velocity streamlines. The method reported in Ref [16] is used to generate Liutex core lines.

3. Structural Visualization

The data source for this study is the real-data analysis of tropical cyclones using the Hurricane Ensemble Data Assimilation System [17], an ensemble Kalman filter-based system that incorporates high-resolution aircraft reconnaissance data along with conventional observations to produce three-dimensional analyses of the atmospheric state. The analyses used here are available at approximately 1 km horizontal resolution and at 44 pressure levels from the surface to 50 hPa in the vertical.

The wind data are presented as three orthogonal wind directions (zonal, meridional, and vertical) on a regularly spaced latitude–longitude grid in the horizontal, and on constant pressure surfaces in the vertical. Horizontal distances are calculated using the standard great circle distance equation. Geopotential height is also available at each grid point, allowing accurate calculation of vertical distances between points. Therefore, all nine velocity gradients can be calculated in units of seconds, and Q, λ_2 and the Liutex vector can thus be calculated. In this study, the color range is selected for Liutex first, and then squared for Q and λ_2, since the unit for Liutex is s^{-1}, and those for Q and λ_2 are s^{-2}.

Analyses of Hurricanes Teddy (2020) and Dorian (2019) are presented to illustrate the application of the vortex identification methods to tropical cyclone structure. Hurricane Teddy formed on 12 September 2020, and intensified rapidly into a major hurricane with a maximum sustained surface wind speed of 140 mph (220 km/h) and a minimum pressure of 945 hPa on 17 September. It became an extratropical cyclone when it approached Canada on 23 September and eventually dissipated on 24 September [18]. Hurricane Dorian formed on 24 August 2019, became a hurricane on 28 August, and intensified rapidly into a Category 5 hurricane with a maximum sustained surface wind speed of 185 mph (295 km/h) and a minimum pressure of 910 hPa on 1 September. After it made landfall in the Bahamas and weakened, Dorian moved northeastward and became an extratropical cyclone on 7 September in Canada before it finally dissipated on 10 September near Greenland [19]. Views of both hurricanes near the times of interest are shown for reference in Figure 1.

Figure 2 shows horizontal views of the various vortex identification methods for one time from Hurricane Teddy at 930 hPa, the model level closest to the standard 925 hPa pressure level, along with the horizontal wind speed and total cloud coverage (TCC, a proxy for the location of convective and stratiform clouds). The methods show the general structure of the three regions (eye, eyewall, and rainbands), but large differences are seen between them. The vector quantities (vorticity and Liutex) can distinguish between horizontal and vertical features and visualize structures in three dimensions that are not entirely in one plane. The eyewall is generally located at the inside edge of the high wind speed gradient (shear) region and is characterized by convective clouds. Because of this high-shear region, the vertical vorticity, in this case a ring, is two orders of magnitude larger than Liutex there. Judging from the figure and compared to horizontal vorticity, it seems that Q removed some of the effect of shear, but the shape of the eye and eyewall also

disappeared. For the λ_2 method, the eye and eyewall are visible, but the direction of the rotation is unknown.

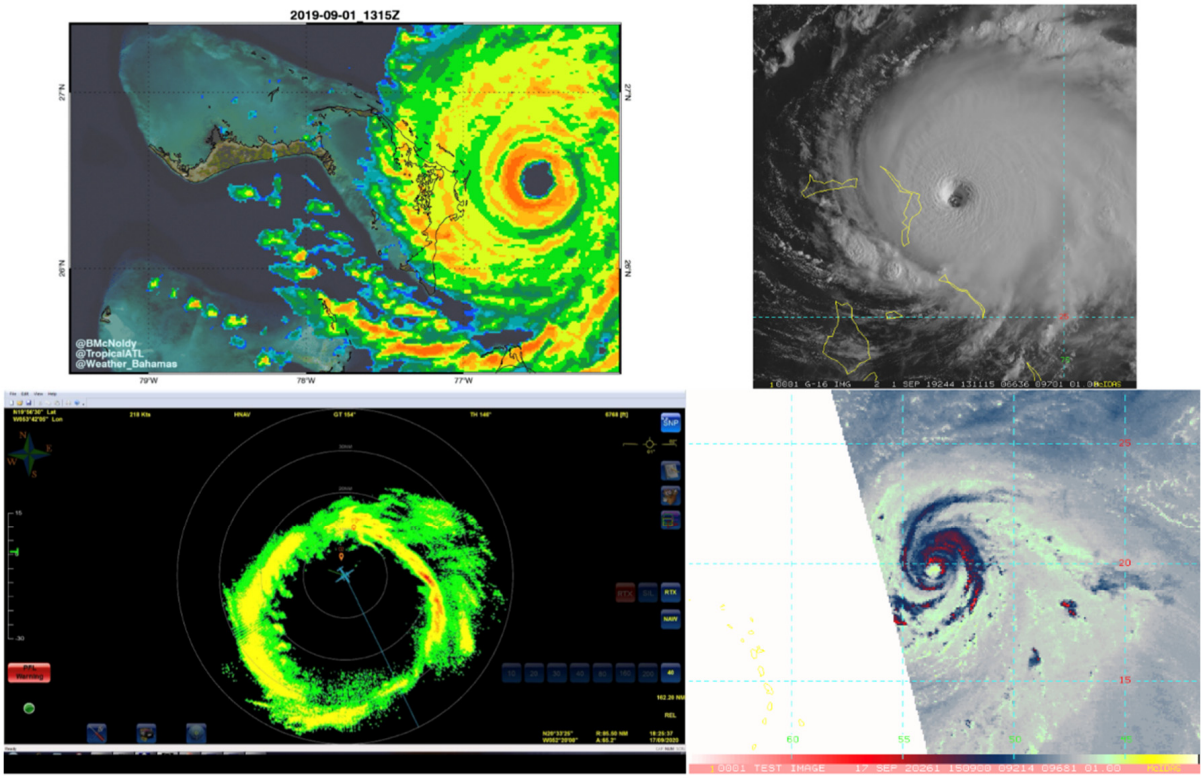

Figure 1. (**upper left**) Single-scan radar reflectivity of Hurricane Dorian from ground-based radar at 1315 UTC 1 September 2019, courtesy Bahamas Department of Meteorology and Brian McNoldy; (**upper right**) visible imagery of Hurricane Dorian from the Geostationary Operational Environmental Satellite East at 1311 UTC on 1 September 2019; (**lower left**) single-scan radar reflectivity of Hurricane Teddy from the multi-mode radar aboard the NOAA WP-3D aircraft at 1825 UTC on 17 September 2020; and (**lower right**) Advanced Microwave Scanning Radiometer 2 89 GHZ imagery of Hurricane Teddy at 1509 UTC 17 September 2020.

Horizontal Liutex reveals localized horizontal vortical structures within the rainband regions. Such structures are associated with variations in vertical and horizontal motion and may include boundary layer roll-like circulations; their detailed dynamical origin is beyond the scope of the present visualization study.

In Figure 3, we set the maximum color range to be 10% of the original for the right two subfigures, and, compared with the left two subfigures, we can find that R_z still present a pattern of concentrating in a central circle, but ζ expands to a wider size, and the eye and eyewall are no longer visible.

Figure 4 shows the three-dimensional Liutex core lines, the local axes of rotation, with the color along each line indicating the local Liutex magnitude and thus the local rigid-rotation strength. At 16:30 UTC on 17 September 2020, the core lines formed a dense, azimuthally organized network that extended upward and outward within the eyewall, with additional filamentary structures extending into the surrounding circulation. The spatial distribution and magnitudes of these lines changed over time, while segments with larger Liutex magnitude remained concentrated mainly within and near the eyewall region. The core lines indicate that the strongest rotational structures within the eyewall are concentrated on the western side, consistent with the location of the strongest eyewall winds, and that the core of Teddy is asymmetric at this time. There are hints that the

eyewall is composed of counter-rotating features, but these may not be clearly represented at the analysis resolution.

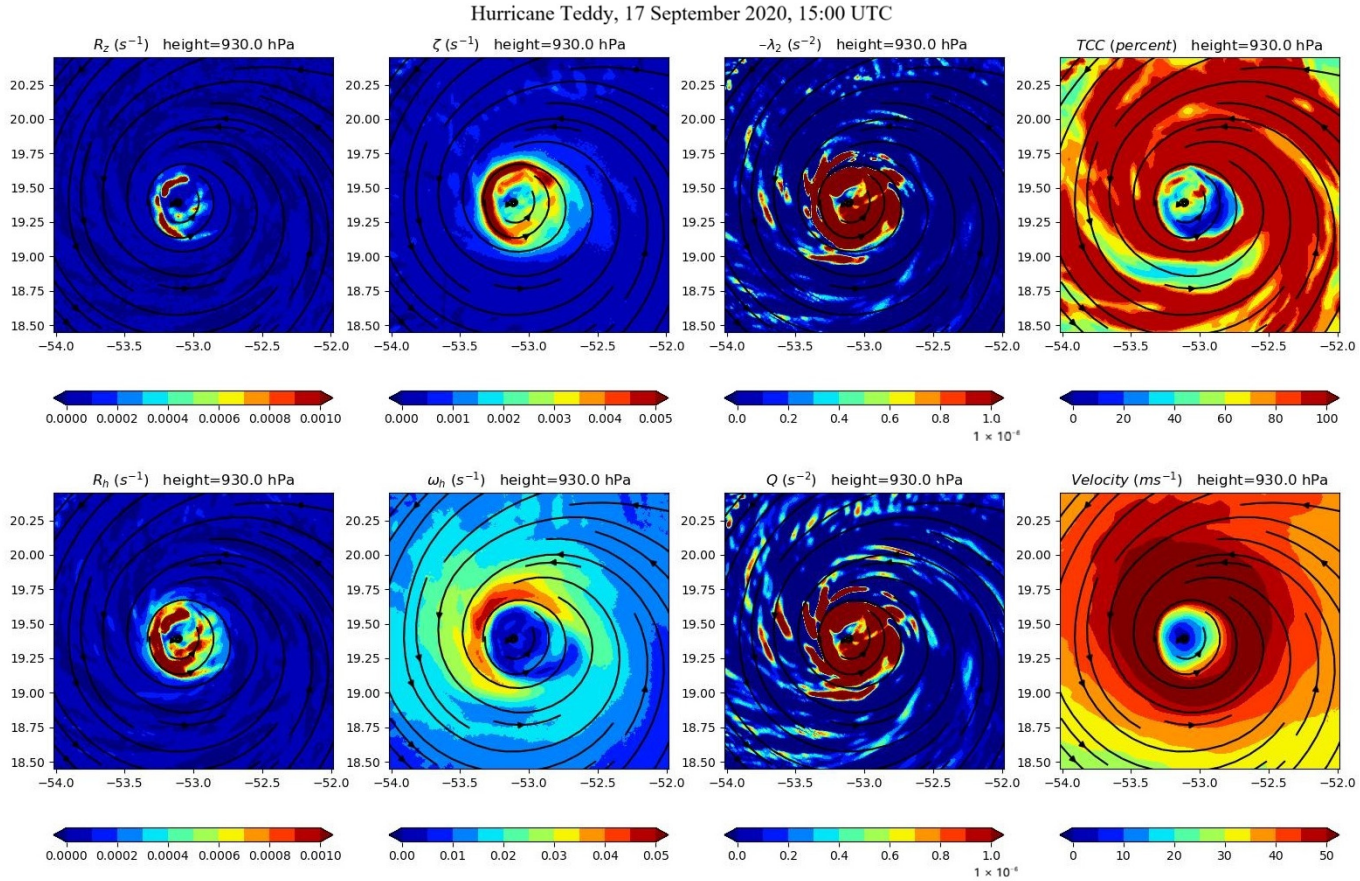

Figure 2. The contour maps of vertical and horizontal Liutex (R_z, R_h), vertical and horizontal vorticity (ζ, ω_h), λ_2 method, Q criterion, total cloud cover (TCC), and horizontal velocity magnitude, with streamlines of horizontal velocity for Hurricane Teddy on 17 September 2020, at 15:00 UTC at the 930 hPa pressure level.

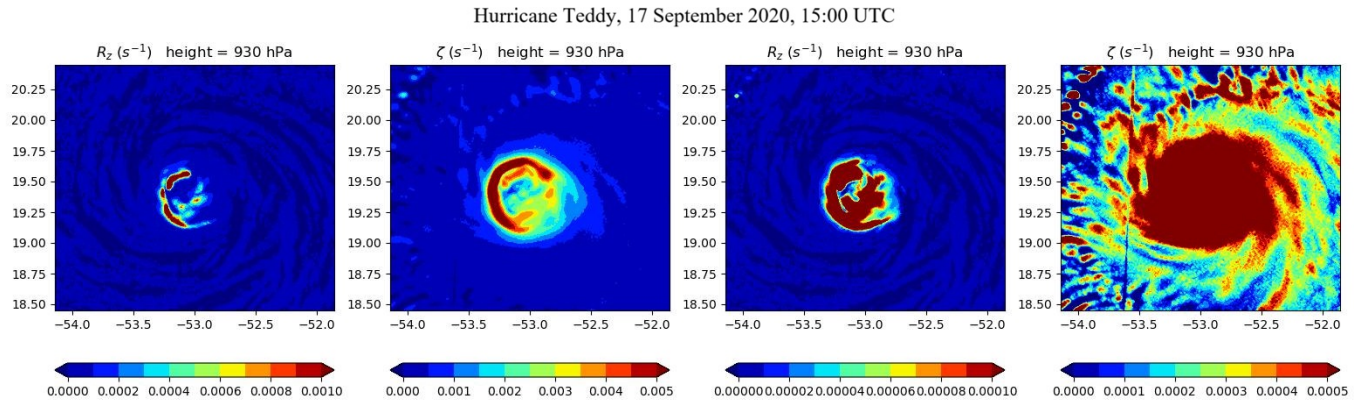

Figure 3. The contour maps of the z-component of Liutex and vorticity, with different color maps.

Hurricane Dorian (Figure 5) and other cases show similar patterns to those seen in Hurricane Teddy except that the inner-core vorticity, λ_2, and Q criterion are all represented by a monopole. The eye and eyewall are still well-represented by the horizontal and vertical Liutex.

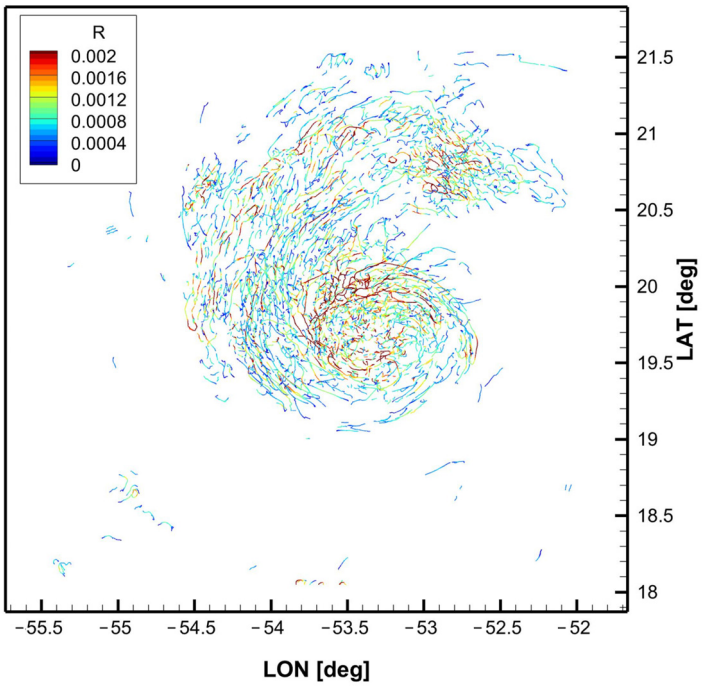

Figure 4. Liutex core lines obtained from the Hurricane Teddy dataset on 17 September 2020 at 16:30. The core lines reveal a dense, asymmetric network of coherent rotational structures around the eye and extending into the surrounding circulation. Core lines are colored by the Liutex magnitude, R, from 0 to 0.002, as indicated by the scale.

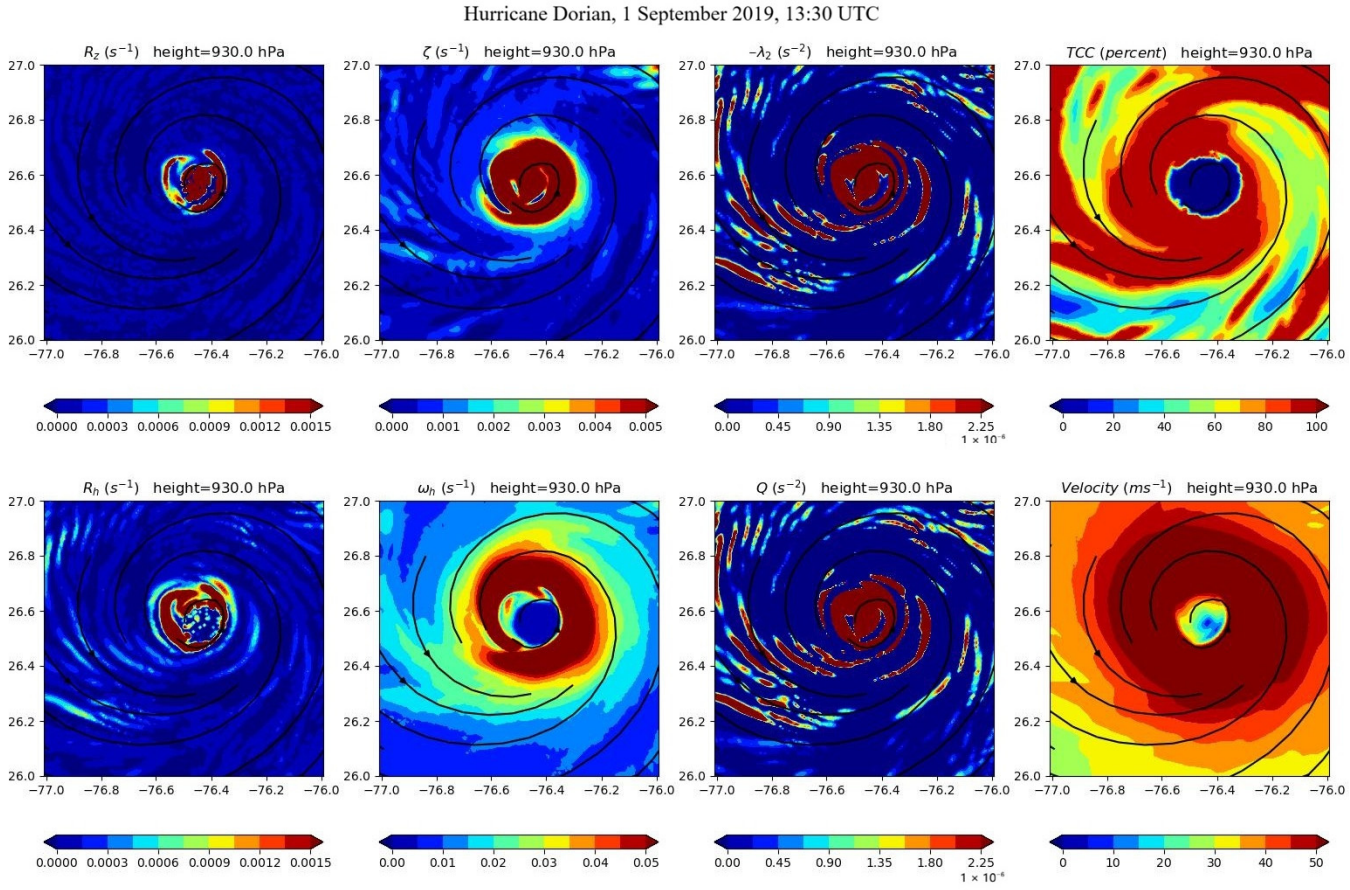

Figure 5. As in Figure 2, except for Hurricane Dorian on 1 September 2019, at 13:30 UTC at the 930 hPa pressure level.

Liutex again suggests that the eyewall consists of numerous coherent vortices rather than a single continuous vortex ring, and that the rainbands can be represented by vortical structures in the vertical direction. This study only compares the representation of tropical cyclone structures using various techniques. Additional research on the processes responsible for their organization and their importance in tropical cyclone structural changes is ongoing.

4. Conclusions

This study provides a case demonstration evaluating the capability of the three generations of vortex identification methods in visualizing structures within tropical cyclones. Only the vector techniques (vorticity and Liutex) can provide the direction and the three-dimensional structure of the features, and all the techniques show varying amounts of the structures of the eye, eyewall, and rainbands. Liutex alone provides complementary structural information suggesting that the eyewall and rainbands are composed of numerous interacting localized vortices rather than a single continuous vortex ring or line. It also shows that vortical structures in rainbands may result from vertical features. These findings provide new perspectives on the organization of tropical cyclone vortex structures.

Beyond visualization, Liutex provides a physically meaningful representation of local rigid body rotation by separating rotational motion from shear. Unlike conventional scalar vortex diagnostics, its vector nature preserves both the magnitude and direction of local rotation, offering additional information for characterizing the spatial organization and evolution of tropical cyclone vortices. Horizontal Liutex reveals localized horizontal vortical structures within the rainband regions. Such structures are associated with variations in vertical and horizontal motion and may include boundary layer roll-like circulations; their detailed dynamical origin is beyond the scope of the present visualization study.

Future studies should further evaluate the performance of Liutex using higher-resolution numerical simulations and real-time cases to assess its robustness and applicability under a wide range of conditions. The framework can also be used to examine the evolution of these structures, their impact on the interaction between the atmosphere and the ocean, and the interaction between the atmosphere and land, which may lead to varying damage impacts by location. The relationship between these structures and intensity change will also be examined. The Liutex framework may also provide new opportunities for investigating coherent vortex structures in other atmospheric, oceanic, and engineering flows where complex rotational motions play a fundamental role.

Author Contributions: Conceptualization, C.M., Y.Y., S.D.A., J.A.Z. and C.L.; methodology, C.M. and Y.Y.; writing—original draft preparation, C.M.; writing—review and editing, S.D.A., J.A.Z., Y.Y. and C.L.; initiative and advice, C.L. and S.D.A.; funding acquisition, Y.Y. and C.L. All authors have read and agreed to the published version of the manuscript.

Funding: This research was funded by NSF, grant #2532216 and #2532217.

Institutional Review Board Statement: Not applicable.

Informed Consent Statement: Not applicable.

Data Availability Statement: The real data analyses used in this study are available at https://www.aoml.noaa.gov/ftp/hrd/aberson/HEDASanalyses/, and accessed on 13 February 2026. The visualization code will be made available by the authors on request.

Acknowledgments: The authors are grateful to NSF for providing research grants #2532216 and #2422573. During the preparation of this manuscript/study, the author(s) used ChatGPT 5.6 SOL for the purposes of checking grammar and typos. The authors have reviewed and edited the output and take full responsibility for the content of this publication.

Conflicts of Interest: The authors declare no conflict of interest.

References

1. Aberson, S.D.; Black, M.L.; Black, R.A.; Burpee, R.W.; Cione, J.J.; Landsea, C.W.; Marks, F.D. Thirty years of tropical cyclone research with the NOAA P-3 aircraft. *Bull. Am. Meteorol. Soc.* **2006**, *87*, 1039–1056. [CrossRef]
2. Kossin, J.P.; Schubert, W.H. Mesovortices, Polygonal Flow Patterns, and Rapid Pressure Falls in Hurricane-Like Vortices. *J. Atmos. Sci.* **2001**, *58*, 2196–2209. [CrossRef]
3. Gao, Y.; Liu, C. Rortex and Comparison with Eigenvalue-Based Vortex Identification Criteria. *Phys. Fluids* **2018**, *30*, 085107. [CrossRef]
4. Liu, C.; Gao, Y.; Tian, S.; Dong, X. Rortex—A New Vortex Vector Definition and Vorticity Tensor and Vector Decompositions. *Phys. Fluids* **2018**, *30*, 035103. [CrossRef]
5. Liu, C.; Gao, Y.; Dong, X.; Wang, Y.; Liu, J.; Zhang, Y.; Cai, X.; Gui, N. Third Generation of Vortex Identification Methods: Omega and Liutex/Rortex Based Systems. *J. Hydrodyn.* **2019**, *31*, 205–223. [CrossRef]
6. Alvarez, O.; Ma, C.; Aberson, S.; Liu, C. Vortex Visualization of Tropical Cyclones by Liutex. *J. Hydrodyn.* **2025**, *37*, 239–245. [CrossRef]
7. von Helmholtz, H. On Integrals of the Hydrodynamic Equations That Correspond to Vortex Motions. *Int. J. Fusion Energy* **1978**, *1*, 41–68.
8. Truesdell, C. *The Kinematics of Vorticity*; Courier Dover Publications: Mineola, NY, USA, 2018.
9. Hunt, J.C.; Wray, A.A.; Moin, P. Eddies, Streams, and Convergence Zones in Turbulent Flows. In *Studying Turbulence Using Numerical Simulation Databases, 2. Proceedings of the 1988 Summer Program*; NASA: Washington, DC, USA, 1988.
10. Jeong, J.; Hussain, F. On the Identification of a Vortex. *J. Fluid Mech.* **1995**, *285*, 69–94. [CrossRef]
11. Chong, M.S.; Perry, A.E.; Cantwell, B.J. A General Classification of Three-dimensional Flow Fields. *Phys. Fluids A Fluid Dyn.* **1990**, *2*, 765–777. [CrossRef]
12. Zhou, J.; Adrian, R.J.; Balachandar, S.; Kendall, T. Mechanisms for Generating Coherent Packets of Hairpin Vortices in Channel Flow. *J. Fluid Mech.* **1999**, *387*, 353–396. [CrossRef]
13. Liu, C.; Yu, Y. Mathematical Foundation of Liutex Theory. *J. Hydrodyn.* **2022**, *34*, 981–993. [CrossRef]
14. Wang, Y.; Gao, Y.; Liu, J.; Liu, C. Explicit Formula for the Liutex Vector and Physical Meaning of Vorticity Based on the Liutex-Shear Decomposition. *J. Hydrodyn.* **2019**, *31*, 464–474. [CrossRef]
15. Gao, Y.; Liu, J.; Yu, Y.; Liu, C. A Liutex Based Definition and Identification of Vortex Core Center Lines. *J. Hydrodyn.* **2019**, *31*, 445–454. [CrossRef]
16. Yu, Y.; Alvarez, O.; Liu, C. A New Automatic Vortex (Liutex) Core Line Identification Method in Boundary-Layer Transition. *Phys. Fluids* **2026**, *38*, 075161. [CrossRef]
17. Aksoy, A.; Aberson, S.D.; Vukicevic, T.; Sellwood, K.J.; Lorsolo, S.; Zhang, X. Assimilation of High-Resolution Tropical Cyclone Observations with an Ensemble Kalman Filter Using NOAA/AOML/HRD's HEDAS: Evaluation of the 2008–11 Vortex-Scale Analyses. *Mon. Weather Rev.* **2013**, *141*, 1842–1865. [CrossRef]
18. Blake, E.S. *"Hurricane Teddy" (PDF). Tropical Cyclone Report*; National Hurricane Center: Miami, FL, USA, 2021.
19. Avila, L.A.; Stewart, S.R.; Berg, R.; Hagen, A.B. *Tropical Cyclone Report. Hurricane Dorian*; National Hurricane Center: Miami, FL, USA, 2020.

Disclaimer/Publisher's Note: The statements, opinions and data contained in all publications are solely those of the individual author(s) and contributor(s) and not of MDPI and/or the editor(s). MDPI and/or the editor(s) disclaim responsibility for any injury to people or property resulting from any ideas, methods, instructions or products referred to in the content.